nature geoscience

LETTERS

PUBLISHED ONLINE: 4 JANUARY 2016 | DOI: 10.1038/NGEO2627

Gradual and sustained carbon dioxide release during Aptian Oceanic Anoxic Event 1a

B. D. A. Naafs[1]*, J. M. Castro[2], G. A. De Gea[2], M. L. Quijano[3], D. N. Schmidt[4] and R. D. Pancost[1]

During the Aptian Oceanic Anoxic Event 1a, about 120 million years ago, black shales were deposited in all the main ocean basins[1]. The event was also associated with elevated sea surface temperatures[2,3] and a calcification crisis in calcareous nannoplankton[4]. These environmental changes have been attributed to variations in atmospheric CO_2 concentrations[2,3,5,6], but the evolution of the carbon cycle during this event is poorly constrained. Here we present records of atmospheric CO_2 concentrations across Oceanic Anoxic Event 1a derived from bulk and compound-specific $\delta^{13}C$ from marine rock outcrops in southern Spain and Tunisia. We find that CO_2 concentrations doubled in two steps during the oceanic anoxic event and remained above background values for approximately 1.5–2 million years before declining. The rise of CO_2 concentrations occurred over several tens to hundreds of thousand years, and thus was unlikely to have resulted in any prolonged surface ocean acidification, suggesting that CO_2 emissions were not the primary cause of the nannoplankton calcification crisis. We find that the period of elevated CO_2 concentrations coincides with a shift in the oceanic osmium-isotope inventory[7] associated with emplacement of the Ontong Java Plateau flood basalts, and conclude that sustained volcanic outgassing was the primary source of carbon dioxide during Oceanic Anoxic Event 1a.

Oceanic anoxic events (OAEs) represent marked changes in the climatic and palaeoceanographic state of the planet. Of these, OAE 1a during the Aptian Stage of the Early Cretaceous period is one of the largest, with black shale deposition in all main ocean basins[1]. Multi-proxy sea surface temperature (SST) estimates from the boreal realm and Pacific Ocean suggest that OAE 1a was accompanied by an approximately 4–8 °C increase in SSTs, assumed to be driven by an increase in p_{CO_2} (refs 2,3). In addition, OAE 1a is concomitant with the calcification crisis of the nannoconids, the most ubiquitous planktic calcifiers during the Early Cretaceous[4]. Their near disappearance is one of the most significant events in the nannoplankton fossil record[8]. Their demise, as well as the malformation and secretion of dwarfed coccoliths and a reduction in pelagic carbonate fluxes, has been suggested to represent a (calcification) response to widespread surface ocean acidification due to an increase in p_{CO_2} (ref. 5). However, the source of excess CO_2, potentially methane release from gas hydrates and/or CO_2 from (submarine) volcanic outgassing, the evolution of p_{CO_2} across OAE 1a, and whether this change in p_{CO_2} is the driving factor for the calcification crisis remains controversial[5–7,9–12]. Most importantly, palaeo-p_{CO_2} proxies have yet to confirm whether changes in p_{CO_2} are indeed associated with these biological and environmental perturbations across OAE 1a and whether surface ocean acidification, defined here as a coupled decline in (surface) ocean pH and Ω (ref. 13) due to rapid input of carbon into the earth system, has happened at all. Determining the relative timing of events is crucial in identifying causal relationships, and can provide crucial constraints for the source of p_{CO_2}, but has been challenging as most records originate from slowly accumulating deep-sea sediments.

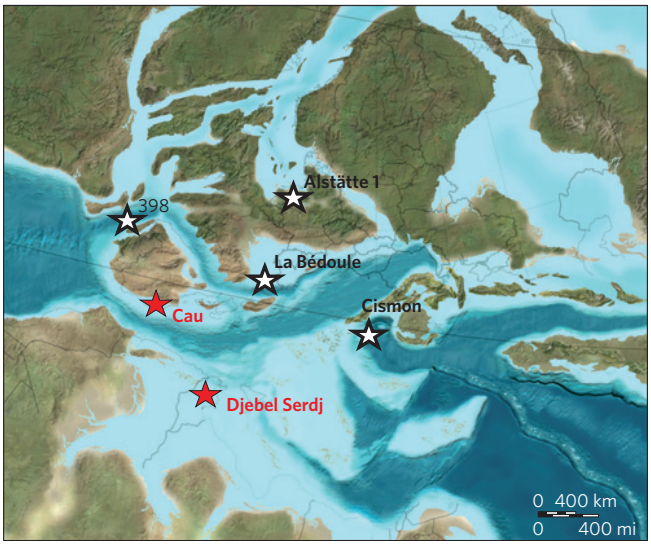

Figure 1 | Study area. Palaeogeographic reconstruction of the Tethys region during the Aptian. The approximated locations of Cau and Djebel Serdj, as well as other key OAE 1a sections, are indicated by red and black stars, respectively. Figure modified from R. Blakey, http://cpgeosystems.com/euromaps.html.

To accurately determine the relative timing, we provide a high-resolution record of p_{CO_2} across OAE 1a from an expanded section in Southern Spain (Cau, Fig. 1). OAE 1a is defined as the interval covering segments C3–C6 and has a thickness of ~40 m at Cau, resulting in an average sedimentation rate of 2.5–4 cm kyr^{-1}, assuming an duration of 1–1.3 Myr (refs 14,15). These sedimentation rates are one order of magnitude higher than those at the OAE 1a reference section at Cismon, but similar to those at other expanded OAE 1a sections[16,17]. The hemipelagic sediments, consisting of marls, marly limestones and black marls (Fig. 2), which contain a rich and well-preserved fossil association, allow a detailed integrated bio- and chemostratigraphy[18,19]. Importantly, the organic matter at Cau is predominantly of marine origin and thermally

[1]Organic Geochemistry Unit, School of Chemistry and Cabot Institute, University of Bristol, Bristol BS8 1TS, UK. [2]Departamento Geología, CEACTierra, University of Jaén, E-23071 Jaén, Spain. [3]Departamento Química Inorgánica y Orgánica, CEACTierra, University of Jaén, E-23071 Jaén, Spain. [4]School of Earth Sciences and Cabot Institute, University of Bristol, Bristol BS8 1RJ, UK. *e-mail: david.naafs@bristol.ac.uk

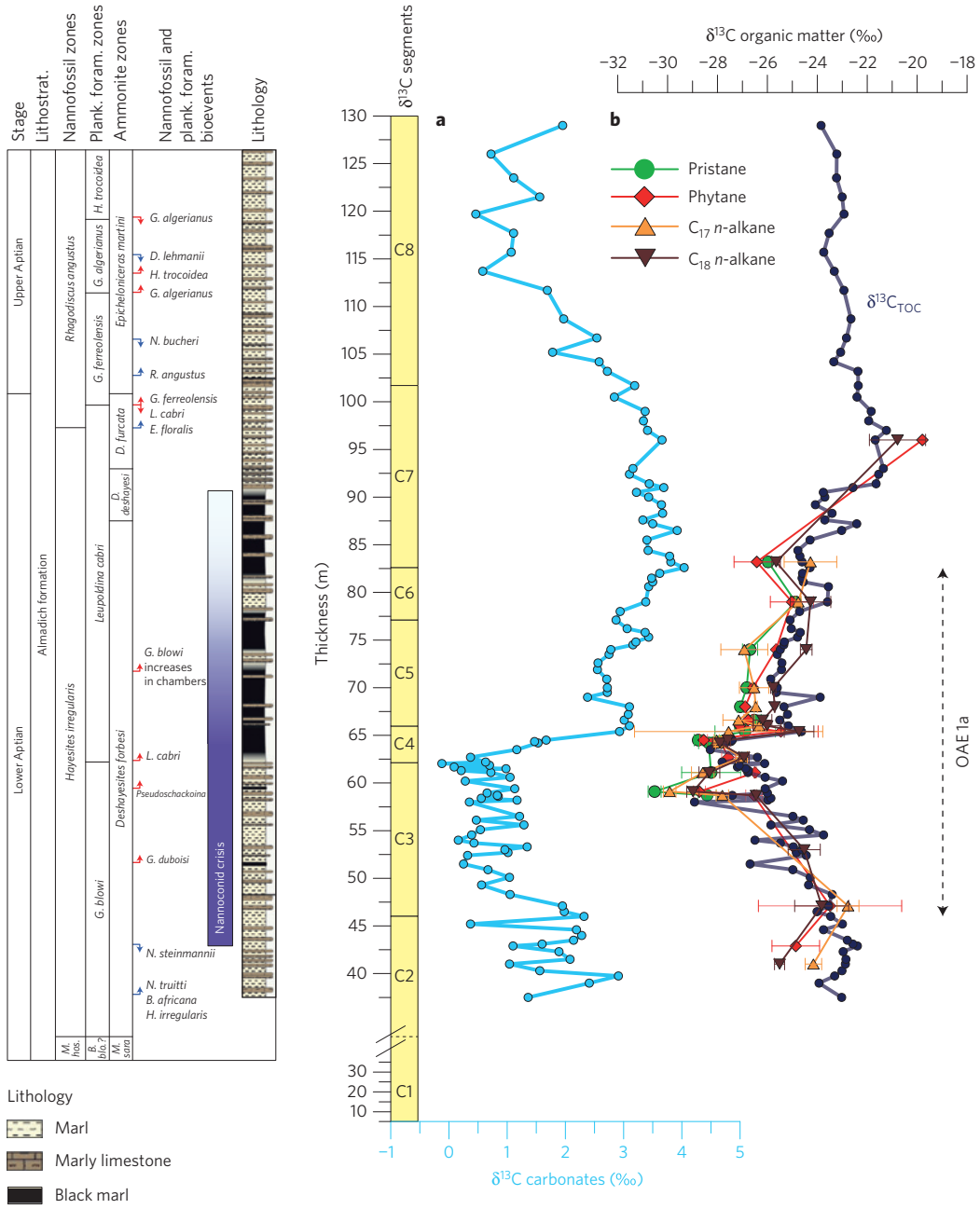

Figure 2 | Carbon-isotope records from Cau across OAE 1a. a,**b**, Lithostratigraphy, biozones, and bioevents at Cau together with bulk carbonate stable carbon isotopes (light blue circles) (**a**) and total organic matter stable carbon isotopes (dark blue circles) together with compound-specific stable carbon isotopes of pristane (green circles), phytane (red diamonds), C_{17} (orange triangles) and C_{18} *n*-alkanes (brown reversed triangles) (**b**). Red arrows refer to planktonic foraminifera, blue arrows refer to calcareous nanofossils, upward arrows represent the first occurrence and downward arrows represent the last occurrence. Error bars on compound-specific stable carbon-isotope data reflect 1σ of replicates. Isotope segments according to Menegatti and colleagues[23]. $\delta^{13}C_{alg}$ is corrected to bulk biomass by adding 4‰.

immature[20]. The nannoconid crisis occurs around 42.5 m in the *Globigerinelloides blowi* planktonic foraminifera zone just before the beginning of the C3 segment and negative C-isotope excursion (NCIE) (refs 18,19), identical to other sections[4,16].

To reconstruct changes in p_{CO_2} we use paired bulk carbonate ($\delta^{13}C_{carb}$) and organic carbon stable carbon isotopes (either bulk organic, $\delta^{13}C_{TOC}$, or based on algal-derived lipids such as pristane, $\delta^{13}C_{alg}$). The difference between these two records, $\Delta^{13}C$ (for example, $\Delta^{13}C_{bulk} = \delta^{13}C_{carb} - \delta^{13}C_{TOC}$), can be used to reconstruct changes in atmospheric CO_2 (ref. 21) and has been applied to reconstruct changes in atmospheric p_{CO_2} throughout Earth's history, including the OAEs (ref. 22). The method relies on the understanding that high p_{CO_2} levels, and hence dissolved CO_2 concentrations in the surface ocean, cause greater discrimination against ^{13}C during algal photosynthesis, leading to more depleted $\delta^{13}C$ values for marine organic matter ($\delta^{13}C_{TOC}$ and $\delta^{13}C_{alg}$) compared to carbonates ($\delta^{13}C_{carb}$). Here, we generate a high-resolution $\Delta^{13}C_{bulk}$ record using $\delta^{13}C_{TOC}$ determined for 114 samples through a 90-m sequence (Fig. 3a).

The $\delta^{13}C_{carb}$ and $\delta^{13}C_{TOC}$ profiles show all eight carbon-isotope segments previously identified to be global[23] that are placed in a tight framework of biostratigraphy[18,19], with the characteristic negative and subsequent positive excursions related to the input of depleted carbon to the ocean–atmosphere and subsequent enhanced carbon

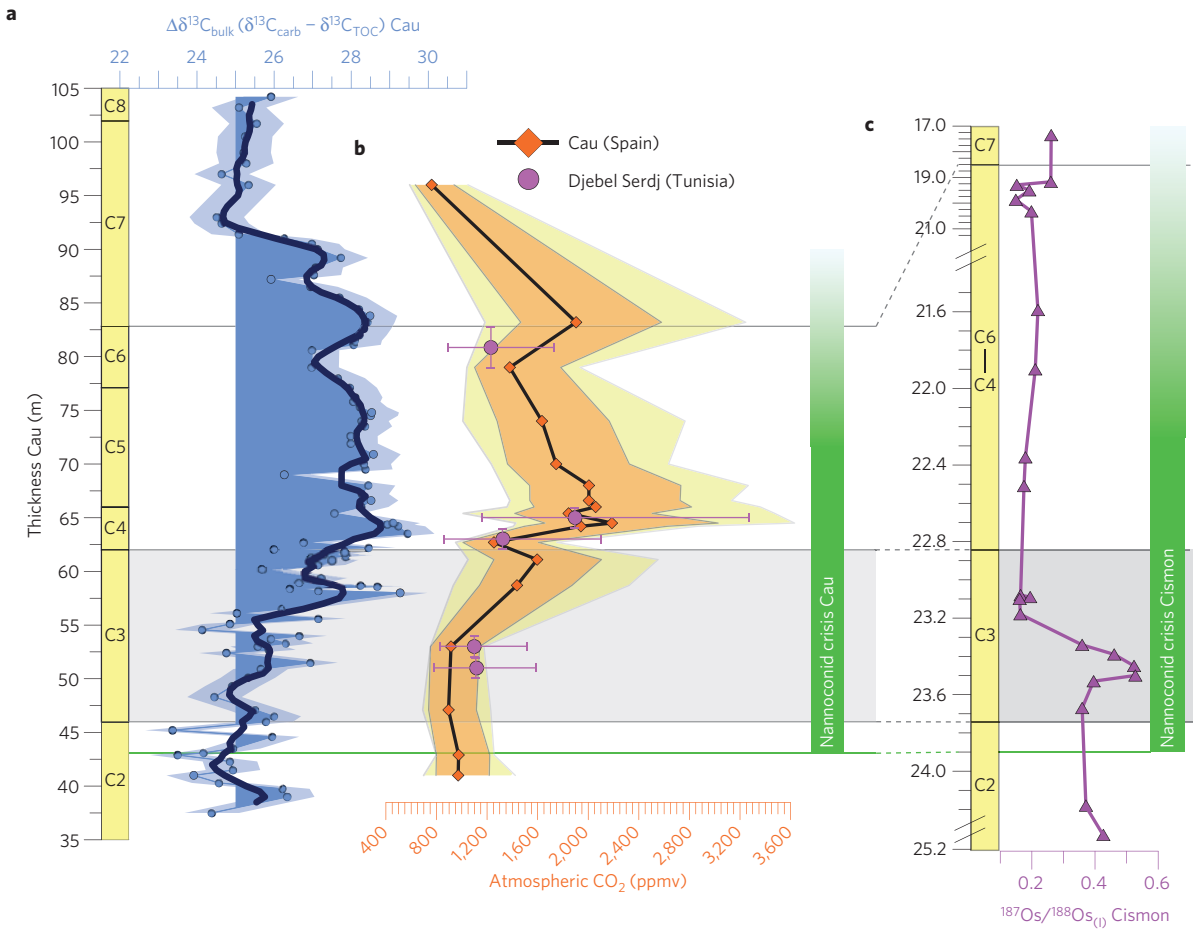

Figure 3 | Estimates of atmospheric CO_2 across OAE 1a. a–c, High-resolution estimates of $\Delta^{13}C_{bulk}$ at Cau (**a**) together with pCO_2 estimates based on $\delta^{13}C_{alg}$ from Cau (orange diamonds) and Djebel Serdj (purple circles) (**b**), and the $^{187}Os/^{188}Os$ record from Cismon[7] (**c**). The duration of the nannoconid crisis at Cau[19] and Cismon[5] is indicated by green bars. Light blue shading in **a** represents uncertainty in $\Delta^{13}C_{bulk}$ and dark blue shading in **a** represents values of $\Delta\delta^{13}C_{bulk}$ in excess of the background value of 25‰. Orange shading in **b** represents the uncertainty in pCO_2 estimates related to uncertainty in $\delta^{13}C_{carb}$ and growth rate and cell geometry (the *b*-value), whereas light-yellow shading is the superimposed spread in the different $\delta^{13}C_{alg}$ for a specific sample. Uncertainty envelopes in **b** are described in the Methods and Supplementary Fig. 7.

burial under global greenhouse conditions (Fig. 2). The absolute values, as well as the overall shape of the $\delta^{13}C_{carb}$ curve, including the magnitude of the positive and negative excursion, are similar to those recorded around the globe (Supplementary Figs 1 and 2).

Biomarkers such as short-chain *n*-alkanes (C_{17} and C_{18}) and pristane and phytane, the latter two derived from phytyl side chains of the chlorophylls of algae and cyanobacteria, can serve as proxies for the isotopic composition of phytoplankton[10,24]. A lower-resolution record of compound-specific $\delta^{13}C$ from Cau was generated using these biomarkers (Fig. 2b), which in our samples predominantly derive from algae ($\delta^{13}C_{alg}$). $\delta^{13}C_{alg}$ was determined for a total of 19 samples and ranges from −24 to −34.5‰ (or −20 to −30.5‰ when corrected to bulk biomass), with the lowest values during the later stage of isotope segments C3 and C4 (Fig. 2b). The shapes and absolute values of $\delta^{13}C_{alg}$ are very similar to $\delta^{13}C_{TOC}$, indicating that $\delta^{13}C_{TOC}$ is not significantly influenced by changes in the composition of bulk organic matter, either through changes in source input or diagenesis. This suggests that the majority of organic matter at Cau is of marine (algal) origin, which is consistent with the overall biomarker assemblage[20].

The $\delta^{13}C_{alg}$ values are also similar to those reported from other (low-resolution) records across OAE 1a. Taken together this demonstrates that the $\delta^{13}C_{alg}$ values we report from Cau are typical for OAE 1a. The similarity of $\delta^{13}C_{alg}$ to other OAE 1a records, together with the absence of major changes in total organic carbon content (Supplementary Fig. 4) and biomarker distribution across OAE 1a, suggests that changes in algal composition (Supplementary Fig. 3), physiology or nutrient contents of the waters are unlikely to have had a significant effect, mitigating concerns associated with growth rate impacts on $\delta^{13}C$ records. The negative shift in $\delta^{13}C_{TOC}$ values, similar to that seen in $\delta^{13}C_{alg}$, and the resulting positive excursion in the $\Delta^{13}C_{bulk}$ record between 55 and 90 m therefore predominantly indicate a greater discrimination against ^{13}C during algal photosynthesis due to elevated p_{CO_2} levels (Fig. 3a).

Using $\delta^{13}C_{alg}$ we then tentatively quantified p_{CO_2} by converting $\Delta^{13}C$ values into ε_p (carbon-isotope discrimination during photosynthesis) and using modern relationships between ε_p and $\{CO_2(aq)\}$. The absolute CO_2 values are calculated using a number of assumptions for palaeoproductivity, sea surface temperature, and equilibrium CO_2 exchange between ocean and atmosphere, and thus should be considered as estimates. Pre-OAE 1a values are estimated as between 800 and 1,200 ppmv (Fig. 3b), entirely consistent with low-resolution multi-proxy estimates of (Early) Cretaceous background p_{CO_2} (refs 13,25). During OAE 1a, specifically the latter part of segment C3–C4, p_{CO_2} doubled to values between 1,400 and 2,800 ppmv. We support the minimum p_{CO_2} values during segment C3 and maximum p_{CO_2} values during segment C4 by providing independent low-resolution p_{CO_2} estimates from the Djebel Serdj section from Tunisia[26] (Fig. 3b). The values, which

were obtained using compound-specific $\delta^{13}C_{alg}$ and the exact same assumptions as used to calculate p_{CO_2} at Cau, range between 1,100 and 2,000 ppmv, with the highest values during C4. The similarity in absolute p_{CO_2} values between the two records demonstrates that the high-resolution p_{CO_2} record from Cau represents a global signal and is not significantly biased by local factors. It is important to note that owing to the nonlinear nature of the relationship between ε_p and $\{CO_2(aq)\}$, the higher p_{CO_2} values could be underestimates.

The p_{CO_2} record for the first time depicts the often-inferred increase and decrease in p_{CO_2} across segments from the later part of C3 to mid-C7 (Fig. 3a,b). As segments C3–C6 (OAE 1a) are estimated to represent around 1.1 Myr and segment C7 a further 1.6 Myr (ref. 15), the period of elevated 'super greenhouse' CO_2 levels probably lasted around 1.5–2 Myr. The continuously high p_{CO_2} values during segments C4–C6 suggest constant input of carbon into the ocean–atmosphere system, almost balanced by extensive organic matter burial in black shales around the world, as indicated by the positive $\delta^{13}C_{carb}$ excursion.

The timing of the p_{CO_2} increase that starts in the middle of segment C3 provides critical constraints on the source of excess CO_2 during OAE 1a. Records from the Pacific and Tethys realms demonstrate that during OAE 1a the global oceanic osmium (Os)-isotope composition was exceptionally unradiogenic (mantle-like), interpreted as reflecting the main phase of eruption of the Ontong Java plateau[7,27]. The major shift in Os isotopes—and hence the eruption phase—occurs well after the onset of the nannoconid crisis during the middle of segment C3, at the same time as the onset of the $\Delta^{13}C_{bulk}/p_{CO_2}$ increase at Cau (Fig. 3c). The simultaneous shifts in Os isotopes and p_{CO_2} provides compelling evidence that the source of excess CO_2 is derived from volcanic outgassing related to the emplacement of the Ontong Java Plateau.

In addition, the initial two-step rise in $\Delta^{13}C_{bulk}/p_{CO_2}$ during segments C3–C4 spans roughly 10 m in our section—from 55 to 65 m (Fig. 3). Estimates from other expanded sections suggest a duration of 100–300 kyr for C3 (refs 16,17), resulting in average sedimentation rates of 5–15 cm kyr^{-1} for this segment. Combined with the assumed duration of segment C4 of 200–280 kyr (ref. 15), the CO_2 doubling took at least 100 kyr, and very likely more than 300 kyr.

Previous studies argued that the nannoconid crisis was caused by widespread and sustained surface ocean acidification due to numerous pulses of CO_2 and methane, with the first pulse coinciding with the onset of the nannoconid crisis during carbon-isotope segment C2 (ref. 5). However, our high-resolution p_{CO_2} record challenges this. Our record indicates a gradual and sustained, two-step increase in p_{CO_2}, probably volcanic sourced, during the latter part of segment C3 and C4, that took place over at least 100 kyr and occurred well after the onset of the nannoconid crisis. Such a slow (>10 kyr) CO_2 release is buffered in the ocean by dissolution of carbonates in deep-sea sediments, combined with silicate rock weathering on land, and, assuming no major spatial shift in carbonate burial, would have prevented a coupled decline in pH and Ω (refs 28,29). Owing to present uncertainties in determining absolute ages or durations in the Early Cretaceous we cannot completely rule out very brief episodes of surface ocean acidification during the latter part of segment C3 and C4, when p_{CO_2} increases. However, the significant lag (~10 m, representing at least 60 kyr during C3) between the onset of the nannoconid crisis and onset of the CO_2 increase and shift in Os isotopes (Fig. 3) clearly demonstrates that CO_2-induced surface ocean acidification could not have caused the nannoconid crisis.

In summary, our records demonstrate that OAE 1a was associated with a gradual, two-step increase in p_{CO_2} to values roughly double the pre-OAE 1a values. The similarity in timing between changes in p_{CO_2} and the oceanic Os-isotope inventory suggests that volcanic outgassing associated with the emplacement of the Ontong Java Plateau was the dominant source of CO_2. The prolonged duration of the p_{CO_2} increase, and by extension the total amount of released carbon, indicates that methane release from gas hydrates was not likely to have been a major source of p_{CO_2} during OAE 1a.

Methods

Methods and any associated references are available in the online version of the paper.

Received 3 September 2015; accepted 1 December 2015; published online 4 January 2016

References

1. Jenkyns, H. C. Geochemistry of oceanic anoxic events. *Geochem. Geophys. Geosyst.* **11,** Q03004 (2010).
2. Mutterlose, J., Bottini, C., Schouten, S. & Sinninghe Damsté, J. S. High sea-surface temperatures during the early Aptian Oceanic Anoxic Event 1a in the boreal realm. *Geology* **42,** 439–442 (2014).
3. Ando, A., Kaiho, K., Kawahata, H. & Kakegawa, T. Timing and magnitude of early Aptian extreme warming: unraveling primary $\delta^{18}O$ variation in indurated pelagic carbonates at Deep Sea Drilling Project Site 463, central Pacific Ocean. *Palaeogeogr. Palaeoclimatol. Palaeoecol.* **260,** 463–476 (2008).
4. Erba, E. Nannofossils and superplumes: the early Aptian 'nannoconid crisis'. *Paleoceanography* **9,** 483–501 (1994).
5. Erba, E., Bottini, C., Weissert, H. J. & Keller, C. E. Calcareous nannoplankton response to surface-water acidification around Oceanic Anoxic Event 1a. *Science* **329,** 428–432 (2010).
6. Méhay, S. *et al.* A volcanic CO_2 pulse triggered the Cretaceous Oceanic Anoxic Event 1a and a biocalcification crisis. *Geology* **37,** 819–822 (2009).
7. Bottini, C., Cohen, A. S., Erba, E., Jenkyns, H. C. & Coe, A. L. Osmium-isotope evidence for volcanism, weathering, and ocean mixing during the early Aptian OAE 1a. *Geology* **40,** 583–586 (2012).
8. Kump, L. R., Bralower, T. J. & Ridgwell, A. Ocean acidification in deep time. *Oceanography* **22,** 94–107 (2009).
9. Gibbs, S. J., Robinson, S. A., Bown, P. R., Jones, T. D. & Henderiks, J. Comment on 'Calcareous nannoplankton response to surface-water acidification around Oceanic Anoxic Event 1a'. *Science* **332,** 175 (2011).
10. Heimhofer, U., Hochuli, P. A., Herrle, J. O., Andersen, N. & Weissert, H. Absence of major vegetation and palaeoatmospheric p_{CO_2} changes associated with Oceanic Anoxic Event 1a (Early Aptian, SE France). *Earth Planet. Sci. Lett.* **223,** 303–318 (2004).
11. van Breugel, Y. *et al.* Synchronous negative carbon isotope shifts in marine and terrestrial biomarkers at the onset of the early Aptian oceanic anoxic event 1a: evidence for the release of ^{13}C-depleted carbon into the atmosphere. *Paleoceanography* **22,** PA1210 (2007).
12. Beerling, D. J., Lomas, M. R. & Gröcke, D. R. On the nature of methane gas-hydrate dissociation during the Toarcian and Aptian Oceanic anoxic events. *Am. J. Sci.* **302,** 28–49 (2002).
13. Hönisch, B. *et al.* The geological record of ocean acidification. *Science* **335,** 1058–1063 (2012).
14. Li, Y.-X. *et al.* Toward an orbital chronology for the early Aptian Oceanic Anoxic Event (OAE1a, ~120 Ma). *Earth Planet. Sci. Lett.* **271,** 88–100 (2008).
15. Malinverno, A., Erba, E. & Herbert, T. D. Orbital tuning as an inverse problem: chronology of the early Aptian Oceanic Anoxic Event 1a (Selli Level) in the Cismon APTICORE. *Paleoceanography* **25,** PA2203 (2010).
16. Kuhnt, W., Holbourn, A. & Moullade, M. Transient global cooling at the onset of early Aptian Oceanic Anoxic Event (OAE) 1a. *Geology* **39,** 323–326 (2011).
17. Lorenzen, J. *et al.* A new sediment core from the Bedoulian (Lower Aptian) stratotype at Roquefort-La Bédoule, SE France. *Cretac. Res.* **39,** 6–16 (2013).
18. de Gea, G. A., Castro, J. M., Aguado, R., Ruiz-Ortiz, P. A. & Company, M. Lower Aptian carbon isotope stratigraphy from a distal carbonate shelf setting: the Cau section, Prebetic zone, SE Spain. *Palaeogeogr. Palaeoclimatol. Palaeoecol.* **200,** 207–219 (2003).
19. Aguado, R., Castro, J. M., Company, M. & Alfonso De Gea, G. Aptian bio-events—an integrated biostratigraphic analysis of the Almadich Formation, Inner Prebetic Domain, SE Spain. *Cretac. Res.* **20,** 663–683 (1999).
20. Quijano, M. L. *et al.* Organic geochemistry, stable isotopes, and facies analysis of the Early Aptian OAE—New records from Spain (Western Tethys). *Palaeogeogr. Palaeoclimatol. Palaeoecol.* **365–366,** 276–293 (2012).
21. Kump, L. R. & Arthur, M. A. Interpreting carbon-isotope excursions: carbonates and organic matter. *Chem. Geol.* **161,** 181–198 (1999).
22. Jarvis, I., Lignum, J. S., Gröcke, D. R., Jenkyns, H. C. & Pearce, M. A. Black shale deposition, atmospheric CO_2 drawdown, and cooling during the Cenomanian–Turonian Oceanic Anoxic Event. *Paleoceanography* **26,** PA3201 (2011).

23. Menegatti, A. P. *et al.* High-resolution $\delta^{13}C$ stratigraphy through the Early Aptian 'Livello Selli' of the Alpine Tethys. *Paleoceanography* **13,** 530–545 (1998).
24. Sinninghe Damsté, J. S., Kuypers, M. M. M., Pancost, R. D. & Schouten, S. The carbon isotopic response of algae, (cyano)bacteria, archaea and higher plants to the late Cenomanian perturbation of the global carbon cycle: insights from biomarkers in black shales from the Cape Verde Basin (DSDP Site 367). *Org. Geochem.* **39,** 1703–1718 (2008).
25. Royer, D. L., Pagani, M. & Beerling, D. J. Geobiological constraints on Earth system sensitivity to CO_2 during the Cretaceous and Cenozoic. *Geobiology* **10,** 298–310 (2012).
26. Heldt, M., Bachmann, M. & Lehmann, J. Microfacies, biostratigraphy, and geochemistry of the hemipelagic Barremian–Aptian in north-central Tunisia: influence of the OAE 1a on the southern Tethys margin. *Palaeogeogr. Palaeoclimatol. Palaeoecol.* **261,** 246–260 (2008).
27. Tejada, M. L. G. *et al.* Ontong Java Plateau eruption as a trigger for the early Aptian oceanic anoxic event. *Geology* **37,** 855–858 (2009).
28. Ridgwell, A. & Schmidt, D. N. Past constraints on the vulnerability of marine calcifiers to massive carbon dioxide release. *Nature Geosci.* **3,** 196–200 (2010).
29. Uchikawa, J. & Zeebe, R. E. Examining possible effects of seawater pH decline on foraminiferal stable isotopes during the Paleocene–Eocene Thermal Maximum. *Paleoceanography* **25,** PA2216 (2010).

Acknowledgements

B.D.A.N. received funding through a Rubicon fellowship, awarded by the Netherlands Organisation for Scientific Research (NWO). Additional funding came from the advanced ERC grant 'The greenhouse earth system' (T-GRES). J.M.C. and M.L.Q. were funded by University of Jaén fellowships. D.N.S. was funded by a Royal Society URF. R.D.P. and D.N.S. acknowledge the Royal Society Wolfson Research Merit Award. We wish to thank the University of Jaén (CICT) for the use of analytical facilities and NERC for partial funding of the mass spectrometry facilities at the University of Bristol (contract no. R8/H10/63; www.lsmsf.co.uk). M. Heldt is thanked for providing the samples from Djebel Serdj. This work is a contribution of the research projects CGL2009-10329 and CGL2014-55274-P (Spanish Ministry of Science and Technology), 'Episodios de Cambio Climático Global' (Instituto de Estudios Giennenses) and RNM-200 (Junta de Andalucía).

Author contributions

B.D.A.N., D.N.S. and R.D.P. designed the study. J.M.C. and G.A.D.G. generated the stratigraphy, gathered the samples in the field and prepared the samples for bulk stable isotope analyses. M.L.Q. and J.M.C. conducted the biomarker extraction and characterization of samples from Cau. B.D.A.N. performed the biomarker extraction of samples from Djebel Serdj, measured all compound-specific isotope data for Cau and Djebel Serdj, and wrote the manuscript with contributions from all authors.

Additional information

Supplementary information is available in the online version of the paper. Reprints and permissions information is available online at www.nature.com/reprints. Correspondence and requests for materials should be addressed to B.D.A.N.

Competing financial interests

The authors declare no competing financial interests.

Methods

Data collection. The Cau section was completed re-logged and remeasured. Bulk C-isotope analyses of the carbonate fraction ($\delta^{13}C_{carb}$) were carried out at the Stable Isotope Laboratory of the University of Michigan, using a Finnigan MAT Kiel IV preparation device coupled directly to the inlet of a Finnigan MAT 253 triple-collector isotope ratio mass spectrometer. The international carbonate standard NBS-19 was used to calibrate to Vienna PeeDee Belemnite (VPDB), with an average precision of 0.15‰. The C-isotope analyses of the total organic fraction ($\delta^{13}C_{TOC}$) were performed at the Stable Isotope Laboratory (SIDI) of the Universidad Autónoma of Madrid. Samples were treated with 3% HCl for 24 h to remove carbonates and then analysed with a Carlo Erba 1108 elemental analyser coupled to a IRMS VG Isochrom in continuous flow mode. The results were calibrated to the VPDB standard, with a precision better than 0.1‰.

Samples for compound-specific C isotopes ($\delta^{13}C_{alg}$) from Cau were extracted at the University of Jaén. Around 10 g of ground bulk sample was extracted using Dionex automated solvent extraction (ASE) and a mixture of dichloromethane (DCM) and methanol (MeOH) (8:2). The ASE program consisted of three 5-min cycles at 100 °C and 10 atm. The five samples from Djebel Serdj (Tunisia) were extracted at the University of Bristol using Soxhlet apparatus. Between 30 and 40 g of ground bulk sample was extracted with a mixture of DCM and MeOH (2:1) for 24 h. The total lipid extracts of samples from both locations were concentrated and separated into three fractions using silica open column chromatography. Successive elution with 3 ml of hexane, 4 ml hexane/DCM (9:1 v/v) and 4 ml of MeOH resulted in saturated hydrocarbon, aromatic and polar fractions, respectively. Compound-specific $\delta^{13}C$ values of the saturated hydrocarbons were determined using an Isoprime 100 GC-combustion-isotope ratio mass spectrometer (GC-C-IRMS) system at the University of Bristol. Samples were measured in duplicate and $\delta^{13}C$ values were converted to VPDB by bracketing with an in-house gas (CO_2) of known $\delta^{13}C$ value. Instrument stability was monitored by regular analysis of an in-house fatty acid methyl ester standard mixture; long-term precision is ±0.3‰. Injection volume was 2 µl onto to a Zebron-I nonpolar column (50 m × 0.32 mm i.d., 0.10 µm film thickness). The GC oven program was: 70 °C (1 min hold) to 130 °C at 20 °C min^{-1}, then to 300 °C at 4 °C min^{-1}, and a final hold for 25 min at 300 °C. Samples were automatically integrated using the IonVantage software package.

pCO_2 calculations using compound-specific $\delta^{13}C_{alg}$. Popp *et al.*[30,31] demonstrated that for several species of marine phytoplankton, and assuming that CO_2(aq) enters the cell via diffusion only, which is likely during the high-CO_2 world of the Cretaceous[32], the isotopic effect associated with the photosynthetic fixation of carbon (ε_p) depends on the concentration of CO_2(aq), the growth rate and the cell geometry.

$$\varepsilon_p = \varepsilon_f - \frac{b}{[CO_2(aq)]} \quad (1)$$

with b being the combined species-specific factors that reflect physiological factors, including growth rate and cell geometry, and ε_f being the maximum isotopic fractionation associated with the photosynthetic fixation of carbon, which is 25‰ for algae[33].

Assuming surface waters were in equilibrium with the atmosphere, atmospheric p_{CO_2} can be calculated using Henry's law:

$$pCO_2(\text{ppmv}) = \frac{[CO_2(aq)]}{K_o} \quad (2)$$

with K_o, the solubility constant, depending on temperature and salinity according to

$$\ln K_o(\text{moles/l/atm}) = A_1 + A_2\frac{100}{T} + A_3\ln\frac{T}{100} + S\left[B_1 + B_2\frac{T}{100} + B_3\left(\frac{T}{100}\right)^2\right] \quad (3)$$

with T = temperature (K), S = salinity (‰), $A_1 = -58.0931$, $A_2 = 90.5069$, $A_3 = 22.2940$, $B_1 = 0.027766$, $B_2 = -0.025888$, $B_3 = 0.0050578$ (ref. 34).

Based on this model, a large number of studies have used bulk organic matter ($\delta^{13}C_{TOC}$) and compound-specific $\delta^{13}C$ values to calculate ε_p and/or p_{CO_2} throughout geologic time[35–39], including the Cretaceous and the OAEs (refs 6,10,22,24,40,41).

Here we calculated p_{CO_2} using $\delta^{13}C_{alg}$ based on four different marine biomarker lipids (C_{17} and C_{18} *n*-alkanes and pristane and phytane) to generate a high-resolution record from Cau and a low-resolution record at Djebel Serdj. Biomarkers such as pristane and phytane, derived from phytol side chains of the chlorophylls of algae and cyanobacteria, are robust proxies for the isotopic composition of phytoplankton[10,42].

ε_p depends on the isotopic difference between dissolved (aq) CO_2 (δ_d) and primary photosynthate (δ_p; ref. 40).

$$\varepsilon_p = 10^3\left[\frac{\delta_d + 1000}{\delta_p + 1000} - 1\right] \quad (4)$$

We calculated the isotopic composition of primary photosynthate (δ_p) using the compound-specific isotopic composition ($\delta^{13}C_{alg}$) and taking into the isotopic offset between biomarker lipids and biomass ($\Delta\delta$), which is assumed to be 4‰ for pristane and phytane[24,41–43]. In our samples $\delta^{13}C$ values of the short-chain *n*-alkanes are very similar to those of pristane and phytane (average offset 0.4‰), in line with findings from other OAEs (ref. 44), and we therefore assumed $\Delta\delta$ to be 4‰ for all four compounds.

$$\delta_p = \delta^{13}C_{TOC} = \delta^{13}C_{alg} + \Delta\delta = \delta^{13}C_{alg} + 4‰ \quad (5)$$

The isotopic composition of dissolved CO_2 (δ_d) was calculated using the isotopic composition of bulk carbonate ($\delta^{13}C_{carb}$), the calcite-bicarbonate enrichment of 1‰ (ref. 45) and the temperature-dependent carbon isotopic fractionation of dissolved CO_2 with respect to HCO_3^- ($\varepsilon_{b(a)}$; ref. 46).

$$\delta_d = \delta^{13}C_{carb} - 1 + \varepsilon_{b(a)} \quad (6)$$

$$\varepsilon_{b(a)} = 24.12 - \frac{9866}{T} \quad (7)$$

Uncertainties in pCO_2 estimates. The absolute CO_2 values are calculated using a number of assumptions for palaeoproductivity, sea surface temperature, and equilibrium CO_2 exchange between ocean and atmosphere, and thus should be considered as estimates. Below we discuss these assumptions and their impact on the absolute p_{CO_2} estimates. Importantly, our main conclusions depend on the timing of changes in p_{CO_2} and are valid independent of the absolute CO_2 estimates or magnitude of change.

Fidelity of the bulk $\delta^{13}C_{carb}$. The first assumption is that bulk $\delta^{13}C_{carb}$ at Cau reflects the isotopic composition of dissolved (aq) CO_2 (δ_d), which directly impacts ε_p (see equations (4) and (6)). First, the $\delta^{13}C$ composition of carbonate rocks is much more resistant to chemical overprinting than $\delta^{18}O$, such that even clearly diagenetically altered and dolomitized carbonates seem to preserve their original $\delta^{13}C$ composition[47], including OAE 1a sections[48]. In addition, nannofossil-dominated bulk carbonate $\delta^{13}C$ is a reliable recorder of $\delta^{13}C_{DIC}$ in pre-Cenozoic sediments[49] and $\delta^{13}C_{carb}$ is well-suited for global correlation during OAEs (ref. 3). As a result, the shape of the $\delta^{13}C_{carb}$ curves and magnitude of the positive and negative carbon-isotope excursion across OAE 1a are similar across the globe (and in a range of depositional settings). In fact, because black shale deposition is asynchronous, most authors use $\delta^{13}C$ chemostratigraphy and the C-isotope segments defined by Menegatti *et al.*[23] to correlate OAE 1a records across the globe[1,14,15,48,50]. Published $\delta^{13}C_{carb}$ records may seem different in shape and magnitude, but this apparent difference between sections is to a large extent due to visual comparison of expanded to condensed sections.

To demonstrate that our $\delta^{13}C_{carb}$ record from Cau is similar in shape and magnitude of excursions to other records, we compare the record from Cau to the $\delta^{13}C_{carb}$ of a similarly expanded section from southeast France[16] (Supplementary Fig. 1). The reason for choosing this record is that it is one of the few other expanded OAE 1a sections. We subsequently tuned the $\delta^{13}C_{carb}$ from the SE France record to the one from Cau other using four tie points. Three are based on biostratigraphy and one on the boundary of the C4/C5-isotope segment. Supplementary Fig. 2 clearly demonstrates the similarity in shape and magnitude of excursion of the two $\delta^{13}C_{carb}$ curves. The similarity between the two $\delta^{13}C_{carb}$ curves, located around 1,000 km apart, suggests that the $\delta^{13}C_{carb}$ record from Cau is not significantly influenced by diagenesis or other secondary effects, but reflects a $\delta^{13}C_{DIC}$ signal and can be used to calculate δ_d. Even so, we assume a 0.5‰ uncertainty in this in our uncertainty estimates (see further below).

Changes in algal composition and physiology. Changes in the algal composition or physiology can affect $\delta^{13}C_{alg}$ and $\delta^{13}C_{TOC}$, and hence ultimately our p_{CO_2} estimates. To assess whether these factors changed across OAE 1a at Cau, we determined the relative C_{27}–C_{30} $\alpha\alpha\alpha$R sterane distribution in all samples. Steranes are derived from algal-derived steroids and sterols, such that their relative distribution in the geologic record is often used to infer changes in algal composition[51,52]. In addition, the sterol, and hence sterane, composition can be influenced by environmental factors such as light intensity, temperature and growth stage[53].

Our results show that the sterane distribution varied little across OAE 1a and changes do not coincide with major changes in $\delta^{13}C$ (Supplementary Fig. 3). This provides strong evidence against significant changes in algal composition and/or environmental factors at Cau during OAE 1a influencing $\delta^{13}C$. This is in line with the lack of a temperature change in the low latitudes during OAE 1a, as indicated by our TEX_{86} estimates from Site 398, as well as the minimal change in TOC content (Supplementary Fig. 4). Taken together, changes in algal composition and/or variations in physiology due to changing environmental factors are unlikely to have had a significant effect. Although more tentative, the lack of any change in algal assemblage suggests that there were no marked changes in the nutrient

contents of the waters, mitigating concerns associated with growth rate impacts on $\delta^{13}C$ records.

Comparison to published records of $\delta^{13}C_{alg}$ and ε_p. The $\delta^{13}C_{alg}$ values from Cau (as well as Djebel Serdj, Supplementary Fig. 8) are similar to those reported from other (low-resolution) sections across OAE 1a. Van Breugel *et al.*[11] provide $\delta^{13}C$ of pristane across part of OAE 1a at Cismon. Their values range between −28 and −35‰, similar to the values we measured at Cau (−29 to −34.5‰ for pristane) and the low-resolution record of Djebel Serdj (−29.2 to −32.6‰ for pristane). For the past 50 Myr, numerous biomarker-based p_{CO_2} records are based on $\delta^{13}C$ of alkenones[35,37]. Although alkenones are generally not found in Cretaceous sediments, the first occurrence of alkenones is actually in the extremely organic rich OAE 1a section at Shatsky Rise (ODP Site 1213; ref. 54). The isotopic composition of these alkenones was determined in one sample (∼−32‰; ref. 55), similar to the minimum values we determined, and again demonstrates that the $\delta^{13}C_{alg}$ values we report are typical for OAE 1a.

None of these studies calculated ε_p. At Shatsky, no $\delta^{13}C_{carb}$ is available. Cismon is characterized by large variations in the source of organic matter[11] and TEX_{86} is influenced by thermal maturity[56]. Heimhofer *et al.*[10] used, among others, C_{17} and C_{18} short-chain *n*-alkanes to reconstruct ε_p across segments C5–C7 in the Serre Chaitieu section from France (Supplementary Fig. 6). For this part of OAE 1a the $\delta^{13}C$ of the short-chain *n*-alkanes in the Serre Chaitieu section ranges between −32 and −27‰, similar to our estimates for these compounds across segments C5–C7 at Cau (−32 to −25‰) and the low-resolution record of Djebel Serdj (−27.9 to −31.8‰). Their estimates of ε_p, although not depicting the increase in p_{CO_2}, as there are no data from segments C3 and C4, with maximumε_p values of around 22‰ are very similar to our maximum ε_p values across this period (maximum ε_p at Cau and Djebel Serdj are ∼22‰ during C4–C6), markedly higher than any values yet to be reported for the past 15 million years[35]. We therefore conclude that our $\delta^{13}C_{alg}$ and ε_p estimates are typical for OAE 1a, and reflect a global signal.

Estimating the *b*-value. The growth rate and cell geometry impact the isotopic effect expressed during the photosynthetic fixation of carbon (ε_p; refs 31,33). These effects are combined into the constant *b* and have an impact on the absolute p_{CO_2} estimates. In the modern ocean, *b* for haptophyte algae ranges from <100 in oligotrophic regions to >200 in upwelling regions[33,57–59].

Although it is not straightforward to estimate *b* during OAE 1a, previous estimates for the Late Cretaceous and OAE 2 assumed a value of 171 (refs 24,41,43). This value is based on the proposed linear correlation between *b* and sedimentary bulk $\delta^{15}N$ values[57] and an assumed $\delta^{15}N$ of −2‰ during the Late Cretaceous at Demerara Rise[41].

$$b = 53.27\left[\frac{\delta^{15}N - 12.386}{-8.146}\right] + 77.21 \quad (8)$$

Bulk $\delta^{15}N$ values across OAE 1a yield similar negative values between −1 and −3‰ (refs 50,60), also suggesting a *b* value of ∼171. This relationship is implicitly based on modern ocean alkenone $\delta^{13}C$ values, and therefore is tuned for coccolithophorids; algae with different surface area to volume ratios or even different membrane diffusivity could have different *b* values[61]. This represents a first-order limitation on the calculation of absolute p_{CO_2} values. Nonetheless, Popp *et al.*[31] have shown that other photoautotrophs do exhibit similar relationships; as such, we can assume a constant *b* value of 171 for our p_{CO_2} estimates, but use a range of *b* values to constrain the uncertainty of the absolute values. Given the lack of evidence for changes in the algal community structure, we suggest that this has had minimal impact on our temporal trends.

Cau was not an upwelling site and is characterized by background TOC values between 0.5 and 1.5%. Even during OAE 1a the period of increased organic matter burial was short lived and not very intense, as indicated by the moderate and brief increase in TOC to maximum values of 2.5% (Supplementary Fig. 4), making it unlikely that the *b* value was much higher. If *b* did increase, then this would have occurred during segments C3–C6, and accounting for it would yield higher p_{CO_2} estimates at this time.

Estimating subtropical sea surface temperatures (SSTs). Sea surface temperatures (SSTs) impact the estimated p_{CO_2} in several ways, but predominantly from their influence on Henry's Law. Here we estimated SSTs using the TEX_{86} palaeothermometer, which is based on the distribution of isoprenoidal glycerol dialkyl glycerol tetraethers (GDGTs) in marine sediments[62,63]. The advantage of TEX_{86} over inorganic geochemical proxies is that TEX_{86} is less influenced by diagenesis, which for example can alter the primary $\delta^{18}O$ signature of carbonates, and is not directly controlled by seawater chemistry such as Mg/Ca and $\delta^{18}O$, which very likely was different during the Cretaceous and especially the OAEs.

We did not detect measurable amounts of GDGTs in the samples from Cau. Although the organic matter at Cau is thermally immature[20] with respect to oil generation, this is not necessarily the case with respect to the occurrence of GDGTs. Owing to the presence of heteroatoms (that is, the ether bond), GDGTs begin to degrade at relatively low thermal maturity[64,65]; in fact, they are uncommon in the maturation window when steranes, pristane and phytane have begun to be liberated from kerogen.

To overcome this issue, we obtained TEX_{86}-based SST estimates from DSDP Site 398 across OAE 1a. Site 398 is located in the North Atlantic, slightly north of Cau (Fig. 1), and covers OAE 1a (ref. 14). Importantly it contains abundant GDGTs. Using the TEX_{86}^H-calibration[66], SSTs at Site 398 across OAE 1a (C3–C6) are remarkably warm and stable, with values around 34.5 °C (Supplementary Fig. 5c). Such high subtropical SSTs are consistent with a large range of proxy evidence that indicates that the Cretaceous was characterized by a hot greenhouse climate[67–70]. In addition, it closely ties in with recent TEX_{86}^H estimates across OAE 1a from the mid-latitudes (∼39° N palaeolatitude) that range between 30 and 33 °C (ref. 2), tropical SSTs in the Pacific that range between 31 and 38 °C during OAE 1a (refs 63,71), and high-latitude Southern Ocean (∼55° N palaeolatitude) SSTs of around 28 °C during OAE 1a (ref. 69), which all indicate very high SSTs during OAE 1a, with SSTs >30 °C extending far into the mid-latitudes.

BIT-values, a proxy for the input of soil-derived GDGTs (ref. 72), vary between 0.06 and 0.41, and there is no correlation between BIT-values and SSTs, arguing against a significant influence of terrestrial GDGTs on the TEX_{86}^H estimates. The organic matter at Site 398 across OAE 1a is thermally immature, as indicated by the C_{31} hopane $\beta\beta/(\beta\beta+\beta\alpha+\alpha\beta)$ ratios, which are always greater than 0.5 (Supplementary Fig. 5d).

The reconstructed SSTs from Site 398 indicate a stable and warm subtropical climate, which seems to be inherent to greenhouse climates[73]. Based on the record from Site 398, we assumed that subtropical SSTs across OAE 1a were relatively stable at Cau (34.5 °C). Higher (36 °C) or lower (30 °C) SST estimates would lead to slightly different (max 250 ppmv) CO_2 values (Supplementary Fig. 6). Assuming an increase in SSTs across OAE 1a, as seen in the higher latitudes[2], would result in a slightly more pronounced increase in p_{CO_2} across OAE 1a.

Uncertainty envelopes. As explained above, our best p_{CO_2} estimates assume a *b*-value of 171, that $\delta^{13}C_{carb}$ reflects seawater $\delta^{13}C_{DIC}$, and that SSTs in the subtropics were 34.5 °C. Assuming these parameters, p_{CO_2} was calculated for, where possible, all four biomarkers and an average of these estimates was plotted in Fig. 3 as a black line with orange data points.

To accurately incorporate the main sources of uncertainty in our p_{CO_2} calculations, largely associated with $\delta^{13}C_{DIC}$ determinations from $\delta^{13}C_{carb}$, which has an impact on ε_p, and uncertainty in the *b*-value due to growth rate and cell physiology, which influences the absolute p_{CO_2} estimates, we calculated a minimum and maximum p_{CO_2} scenario. The minimum scenario assumes that $\delta^{13}C_{carb}$ overestimates seawater $\delta^{13}C_{DIC}$ by 0.5‰ and a low-end *b*-value of 150. The maximum scenario assumes that $\delta^{13}C_{carb}$ underestimates seawater $\delta^{13}C_{DIC}$ by 0.5‰ and a high-end *b*-value of 200. Note that uncertainty in $\delta^{13}C_{carb}$ manifests in ε_p, which at Cau is similar compared to previous estimates[10] and other sites. A range from 150 to 200 for *b* was chosen as both Cau and Djebel Serdj are not upwelling sites and not characterized by large variations in TOC content or changes in algal composition and physiology. Assuming these parameters, p_{CO_2} was calculated for all four biomarkers. In Fig. 3 and Supplementary Fig. 8, the orange shading represents the spread between the minimum and maximum p_{CO_2} estimates and, again, is the average value of all biomarker measurements (see Supplementary Fig. 7). The light-yellow shading represents the analytical uncertainty related to the compound-specific $\delta^{13}C$ measurements (for example, how well does the average value of the four biomarkers represent the spread in compound-specific $\delta^{13}C$) and represents 1σ from the average min. and max. p_{CO_2}-scenario (for example 1σ from the orange shading).

The uncertainty in $\Delta^{13}C$ (the turquoise shading in Fig. 3), was calculated assuming both $\delta^{13}C_{carb}$ and $\delta^{13}C_{TOC}$ were as much as 0.5‰ too high or too low compared to seawater $\delta^{13}C_{DIC}$ and primary photosynthate $\delta^{13}C$, respectively, resulting in a combined error of 0.71‰ ($\sqrt{(0.5^2+0.5^2)}$).

Duration of isotope segment C3. Following Menegatti *et al.*[23] we defined C3 to span the decrease in bulk $\delta^{13}C_{carb}$, covering the interval between 46 and 62 m in our section (Fig. 2a). Identical to other OAE 1a records[5,15,16], the onset of the nannoconid crisis precedes the beginning of C3 at Cau. The first occurrence of *Schackoina cabri* at the top of C3 corresponds to what has been observed in other expanded sections[16,17].

Previous estimates for the duration of C3 range from 20 to 45 kyr at Cismon[14,15]. However, results from other more expanded sections demonstrate that this interval in Cismon is (highly) condensed and the duration of C3 was probably longer, with ranges between 100 and 300 kyr (refs 16,17,74,75). Recently the C3 interval at Cismon was also redefined, with an updated duration of between 100 and 200 kyr (ref. 56).

Duration of the reconstructed CO_2 input at Cau. Even assuming a minimal duration of 20–45 kyr for C3, as suggested by the original Cismon estimates[14,15], the reconstructed CO_2 increase at Cau occurs across the later part of C3 as well as the majority of C4, which lasted 239 ± 39 kyr at Cismon[15]. This implies that, independent of the exact duration of C3, the CO_2 increase occurred over at least

100 kyr. Assuming a more likely duration of C3 of 100–300 kyr, together with the duration of C4 of 239 kyr, implies that the CO_2 increase at Cau probably occurred over more than 300 kyr.

Correlations to Cau. We used the carbon-isotope segment chemostratigraphy, originally developed by Menegatti *et al.*[23], to compare the p_{CO_2} record from Djebel Serdj and the Os-isotope record from Cismon against the records from Cau. For Cismon we used the updated definition of isotope segment C3 as used in Bottini and colleagues[56]. For the timing of the nannoconid crisis at Cismon we used the definition given in Malinverno and colleagues[15]. For Djebel Serdj we redefined the carbon-isotope segments as shown in Supplementary Fig. 8, largely following Heldt and colleagues[26]. The low-resolution p_{CO_2} estimates from Djebel Serdj were plotted on top of those of Cau using a direct correlation. So, for example, the estimates from the middle of segment C3 at Djebel Serdj are shown in the middle of C3 at Cau. The vertical error bars on the p_{CO_2} estimates from Djebel Serdj as shown in Fig. 3 represent the uncertainty in this correlation.

References

30. Popp, B. N., Takigiku, R., Hayes, J. M., Louda, J. W. & Baker, E. W. The post-Paleozoic chronology and mechanism of ^{13}C depletion in primary marine organic matter. *Am. J. Sci.* **289,** 436–454 (1989).
31. Popp, B. N. *et al.* Effect of Phytoplankton cell geometry on carbon isotopic fractionation. *Geochim. Cosmochim. Acta* **62,** 69–77 (1998).
32. Laws, E. A., Popp, B. N., Cassar, N. & Tanimoto, J. ^{13}C discrimination patterns in oceanic phytoplankton: likely influence of CO_2 concentrating mechanisms, and implications for palaeoreconstructions. *Funct. Plant Biol.* **29,** 323–333 (2002).
33. Bidigare, R. R. *et al.* Consistent fractionation of ^{13}C in nature and in the laboratory: growth-rate effects in some haptophyte algae. *Glob. Biogeochem. Cycles* **11,** 279–292 (1997).
34. Weiss, R. F. Carbon dioxide in water and seawater: the solubility of a non-ideal gas. *Mar. Chem.* **2,** 203–215 (1974).
35. Pagani, M., Zachos, J. C., Freeman, K. H., Tipple, B. & Bohaty, S. Marked decline in atmospheric carbon dioxide concentrations during the Paleogene. *Science* **309,** 600–603 (2005).
36. Schoon, P. L., Sluijs, A., Sinninghe Damsté, J. S. & Schouten, S. Stable carbon isotope patterns of marine biomarker lipids in the Arctic Ocean during Eocene Thermal Maximum 2. *Paleoceanography* **26,** PA3215 (2011).
37. Seki, O. *et al.* Alkenone and boron-based Pliocene p_{CO_2} records. *Earth Planet. Sci. Lett.* **292,** 201–211 (2010).
38. Badger, M. P. S. *et al.* CO_2 drawdown following the middle Miocene expansion of the Antarctic Ice Sheet. *Paleoceanography* **28,** 42–53 (2013).
39. Raymo, M. E., Grant, B., Horowitz, M. & Rau, G. H. Mid-Pliocene warmth: stronger greenhouse and stronger conveyor. *Mar. Micropaleontol.* **27,** 313–326 (1996).
40. Freeman, K. H. & Hayes, J. M. Fractionation of carbon isotopes by phytoplankton and estimates of ancient CO_2 levels. *Glob. Biogeochem. Cycles* **6,** 185–198 (1992).
41. Bice, K. L. *et al.* A multiple proxy and model study of Cretaceous upper ocean temperatures and atmospheric CO_2 concentrations. *Paleoceanography* **21,** PA2002 (2006).
42. Schouten, S. *et al.* Biosynthetic effects on the stable carbon isotopic compositions of algal lipids: implications for deciphering the carbon isotopic biomarker record. *Geochim. Cosmochim. Acta* **62,** 1397–1406 (1998).
43. van Bentum, E. C., Reichart, G. J., Forster, A. & Sinninghe Damsté, J. S. Latitudinal differences in the amplitude of the OAE-2 carbon isotopic excursion: p_{CO_2} and paleo productivity. *Biogeosciences* **9,** 717–731 (2012).
44. Schouten, S., van Kaam-Peters, H. M. E., Rijpstra, W. I. C., Schoell, M. & Sinninghe Damsté, J. S. Effects of an oceanic anoxic event on the stable carbon isotopic composition of early Toarcian carbon. *Am. J. Sci.* **300,** 1–22 (2000).
45. Romanek, C. S., Grossman, E. L. & Morse, J. W. Carbon isotopic fractionation in synthetic aragonite and calcite: effects of temperature and precipitation rate. *Geochim. Cosmochim. Acta* **56,** 419–430 (1992).
46. Mook, W. G., Bommerson, J. C. & Staverman, W. H. Carbon isotope fractionation between dissolved bicarbonate and gaseous carbon dioxide. *Earth Planet. Sci. Lett.* **22,** 169–176 (1974).
47. Halverson, G. P., Hoffman, P. F., Schrag, D. P., Maloof, A. C. & Rice, A. H. N. Toward a Neoproterozoic composite carbon-isotope record. *Geol. Soc. Am. Bull.* **117,** 1181–1207 (2005).
48. Jenkyns, H. C. in *Proceedings of the Ocean Drilling Program, Scientific Results* Vol. 143 (eds Winterer, E. L., Sager, W. W., Firth, J. V. & Sinton, J. M.) 99–104 (Ocean Drilling Program, 1995).
49. Stoll, H. M. Limited range of interspecific vital effects in coccolith stable isotopic records during the Paleocene–Eocene thermal maximum. *Paleoceanography* **20,** PA1007 (2005).
50. Dumitrescu, M. & Brassell, S. C. Compositional and isotopic characteristics of organic matter for the early Aptian Oceanic Anoxic Event at Shatsky Rise, ODP Leg 198. *Palaeogeogr. Palaeoclimatol. Palaeoecol.* **235,** 168–191 (2006).
51. Grantham, P. J. & Wakefield, L. L. Variations in the sterane carbon number distributions of marine source rock derived crude oils through geological time. *Org. Geochem.* **12,** 61–73 (1988).
52. Schwark, L. & Empt, P. Sterane biomarkers as indicators of palaeozoic algal evolution and extinction events. *Palaeogeogr. Palaeoclimatol. Palaeoecol.* **240,** 225–236 (2006).
53. Volkman, J. Sterols in microorganisms. *Appl. Microbiol. Biotechnol.* **60,** 495–506 (2003).
54. Brassell, S. C. & Dumitrescu, M. Recognition of alkenones in a lower Aptian porcellanite from the west-central Pacific. *Org. Geochem.* **35,** 181–188 (2004).
55. Dumitrescu, M. & Brassell, S. C. Biogeochemical assessment of sources of organic matter and paleoproductivity during the early Aptian Oceanic Anoxic Event at Shatsky Rise, ODP Leg 198. *Org. Geochem.* **36,** 1002–1022 (2005).
56. Bottini, C. *et al.* Climate variability and ocean fertility during the Aptian Stage. *Clim. Past* **11,** 383–402 (2015).
57. Andersen, N., Müller, P. J., Kirst, G. & Schneider, R. R. in *Use of Proxies in Paleoceanography* (eds Fischer, G. & Wefer, G.) Ch. 19, 469–488 (Springer, 1999).
58. Schulte, S., Benthien, A., Andersen, N., Müller, P. J. & Schneider, R. in *The South Atlantic in the Late Quaternary: Reconstruction of Material Budget and Current Systems* (eds Wefer, G., Mulitza, S. & Ratmeyer, V.) 195–211 (Springer, 2003).
59. Pagani, M. The alkenone-CO_2 Proxy and ancient atmospheric carbon dioxide. *Phil. Trans. R. Soc. Lond. A* **360,** 609–632 (2002).
60. Kuypers, M. M. M., van Breugel, Y., Schouten, S., Erba, E. & Sinninghe Damsté, J. S. N_2-fixing cyanobacteria supplied nutrient N for Cretaceous oceanic anoxic events. *Geology* **32,** 853–856 (2004).
61. Pancost, R. D. *et al.* Reconstructing Late Ordovician carbon cycle variations. *Geochim. Cosmochim. Acta* **105,** 433–454 (2013).
62. Schouten, S., Hopmans, E. C., Schefuss, E. & Sinninghe Damsté, J. S. Distributional variations in marine crenarchaeotal membrane lipids: a new tool for reconstructing ancient sea water temperatures? *Earth Planet. Sci. Lett.* **204,** 265–274 (2002).
63. Schouten, S. *et al.* Extremely high sea-surface temperatures at low latitudes during the middle Cretaceous as revealed by archaeal membrane lipids. *Geology* **31,** 1069–1072 (2003).
64. Schouten, S., Hopmans, E. C. & Sinninghe Damsté, J. S. The effect of maturity and depositional redox conditions on archaeal tetraether lipid palaeothermometry. *Org. Geochem.* **35,** 567–571 (2004).
65. Schouten, S., Hopmans, E. C. & Sinninghe Damsté, J. S. The organic geochemistry of glycerol dialkyl glycerol tetraether lipids: a review. *Org. Geochem.* **54,** 19–61 (2013).
66. Kim, J.-H. *et al.* New indices and calibrations derived from the distribution of crenarchaeal isoprenoid tetraether lipids: implications for past sea surface temperature reconstructions. *Geochim. Cosmochim. Acta* **74,** 4639–4654 (2010).
67. Littler, K., Robinson, S. A., Bown, P. R., Nederbragt, A. J. & Pancost, R. D. High sea-surface temperatures during the Early Cretaceous Epoch. *Nature Geosci.* **4,** 169–172 (2011).
68. Jenkyns, H. C., Forster, A., Schouten, S. & Sinninghe Damsté, J. S. High temperatures in the Late Cretaceous Arctic Ocean. *Nature* **432,** 888–892 (2004).
69. Jenkyns, H. C., Schouten-Huibers, L., Schouten, S. & Sinninghe Damsté, J. S. Warm Middle Jurassic–Early Cretaceous high-latitude sea-surface temperatures from the Southern Ocean. *Clim. Past* **8,** 215–226 (2012).
70. Tarduno, J. A. *et al.* Evidence for extreme climatic warmth from Late Cretaceous Arctic vertebrates. *Science* **282,** 2241–2243 (1998).
71. Dumitrescu, M., Brassell, S. C., Schouten, S., Hopmans, E. C. & Sinninghe Damsté, J. S. Instability in tropical Pacific sea-surface temperatures during the early Aptian. *Geology* **34,** 833–836 (2006).
72. Hopmans, E. C. *et al.* A novel proxy for terrestrial organic matter in sediments based on branched and isoprenoid tetraether lipids. *Earth Planet. Sci. Lett.* **224,** 107–116 (2004).
73. Pearson, P. N. *et al.* Stable warm tropical climate through the Eocene Epoch. *Geology* **35,** 211–214 (2007).
74. Hu, X., Zhao, K., Yilmaz, I. O. & Li, Y. Stratigraphic transition and palaeoenvironmental changes from the Aptian Oceanic Anoxic Event 1a (OAE1a) to the Oceanic Red Bed 1 (ORB1) in the Yenicesihlar section, central Turkey. *Cretac. Res.* **38,** 40–51 (2012).
75. Huck, S., Heimhofer, U., Rameil, N., Bodin, S. & Immenhauser, A. Strontium and carbon-isotope chronostratigraphy of Barremian–Aptian shoal-water carbonates: northern Tethyan platform drowning predates OAE 1a. *Earth Planet. Sci. Lett.* **304,** 547–558 (2011).